

Iterative Compression-Decimation Scheme for Tensor Network Optimization

Zhi-Cheng Yang,¹ Stefanos Kourtis,¹ Claudio Chamon,¹ Eduardo R. Mucciolo,² and Andrei E. Ruckenstein¹

¹*Physics Department, Boston University, Boston, Massachusetts 02215, USA*

²*Department of Physics, University of Central Florida, Orlando, Florida 32816, USA*

(Dated: May 15, 2022)

Motivated by statistical physics models connected to computation problems, we devise a tensor network technique that is suited to problems with or without translation invariance and with arbitrary boundary conditions. We introduce a compression-decimation algorithm as an efficient iterative scheme to optimize tensor networks that encode generalized vertex models on regular lattices. The algorithm first propagates local constraints to longer ranges via repeated contraction-decomposition sweeps over all lattice bonds, thus achieving compression on a given length scale. It then decimates the lattice via coarse-graining tensor contractions. Repeated iterations of these two steps allow us to gradually collapse the tensor network while keeping the tensor dimensions under control, such that ultimately the full tensor trace can be taken for relatively large systems. As a benchmark, we demonstrate the efficiency of the algorithm by computing the ground state entropy density of the planar ice model and the eight-vertex model. We then apply it to reversible classical computational problems based on a recently proposed vertex model representation of classical computations [Nat. Commun. **8**, 15303 (2017)]. Our protocol allows us to obtain the exact number of solutions for computations where a naive enumeration would take astronomically long times, suggesting that the algorithm is a promising practical tool for the solution of a plethora of problems in physics and computer science.

I. INTRODUCTION

Physics-inspired approaches have led to efficient algorithms for tackling typical instances of hard computational problems, shedding new light on our understanding of the complexity of such problems [1, 2]. The conceptual framework of these approaches is based on the realization that the solutions of certain computational problems are encoded in ground states of appropriate statistical mechanics models. However, the existence of either a thermodynamic phase transition into a glassy phase or a first-order quantum phase transition represent obstructions to reaching the ground state, often even for easy problems [3–7]. Recently, Ref. [8] introduced a new class of problems by mapping a generic reversible classical computation onto a two-dimensional vertex model with appropriate boundary conditions. The statistical mechanics model resulting from this mapping displays no bulk thermodynamic phase transitions and the bulk thermodynamics is independent of the classical computation represented by the model. Taken together, these features remove an obvious obstacle to reaching the ground state of a large class of computational problems and imply that the time-to-solution and the complexity of the problem are determined by the dynamics of the relaxation of the corresponding system to its ground state. However, when thermal annealing is employed, the resulting dynamics is found to be extremely slow, and even easy computational problems cannot be efficiently solved.

Motivated by the need to find a more efficient way to reach ground-state configurations of vertex models, in this paper we introduce a tensor network approach to general statistical mechanical vertex models and, in particular, to those encoding computational problems. Tensor networks are a powerful tool to study classical and

quantum many-body systems in two and higher spatial dimensions, and are also used as compressed representations of large-scale structured data in “big-data” analytics [9–11]. In our context, we are interested in taking the trace of tensor networks [12–14], which amounts to a computation of the partition function. As opposed to thermal annealing, which serially visits individual configurations, tensor network schemes sum over all configurations simultaneously. As a result, tensor-based approaches lead to a form of virtual parallelization [15], which, under certain circumstances, speeds up the computation of the trace. Most of the physics-driven applications have focused on tensor network renormalization group (TNRG) algorithms that coarse grain the network while optimally removing short-range entanglement [16–28]. While our algorithm can be used to implement the TNRG for physical systems, when applied to computational problems, it must account for two generic complications of computation, namely, non-trivial boundary constraints and lack of translational invariance. Both features are naturally treated by the methods proposed in this paper.

Our tensor network approach, which we refer to as the iterative compression-decimation (ICD) algorithm, can be regarded as a set of local moves defining a novel dynamical path to the ground state of generalized vertex models on a square lattice. These moves can be shown to decrease or leave unchanged the bond dimensions of the tensors involved, thus achieving optimal compression (i.e., minimal bond dimension) of the tensor network on a lattice of fixed size. The algorithm’s first step is to propagate local vertex constraints across the system via repeated contraction-decomposition sweeps over all lattice bonds. These back and forth sweeps are the higher dimensional tensor-network analog of those employed in

the one-dimensional finite-system density matrix renormalization group (DMRG) [29] method. For problems with non-trivial boundary conditions, such as those encountered in computation, these sweeps also propagate the boundary constraints into the bulk, thus progressively building the connection between opposite (i.e., input/output) boundaries. In the next step, the algorithm decreases the size of the lattice by coarse-graining the tensor network via suitable contractions. Repeated iterations of these two steps allow us to reach larger and larger system sizes while keeping the tensor dimensions under control, such that ultimately the full tensor trace can be taken.

We first demonstrate the performance of our algorithm by applying it to two statistical mechanics problems, namely the six- and eight-vertex models. In both cases, we obtain the exact result for the zero-temperature entropy in the thermodynamic limit. We then proceed to study the random TOFFOLI vertex model for reversible classical computations [8]. In this model, the truth table of each vertex constraint corresponding to a computational gate is encoded in a tensor, such that the local compatibility between neighboring bits (or spins) is automatically guaranteed upon contracting the shared bond between two tensors. Summing over all possible unfixed boundary vertex states and contracting the entire tensor network give the partition function, which counts the total number of solutions compatible with the boundary conditions, a problem belonging to the class #P. Finding a solution can then be accomplished by fixing one boundary vertex at a time, with the total number of trials linear in the number of input bits. As already mentioned, this can be viewed as a form of virtual parallelization [15], since the boundary tensors contain all possible states simultaneously in a compact way.

The computational cost of ICD hinges upon the maximum bond dimension of the tensors during the coarse-graining procedure. We identify the hardness of a given counting problem by studying the scaling of the maximum bond dimension as a function of the system size, the concentration of nontrivial constraints imposed by TOFFOLI gates, and the ratio of unfixed boundary vertices. While we cannot distinguish between polynomial and exponential scaling for the hardest regime of high TOFFOLI concentration, there exist certain regimes of the problem where the bond dimension grows relatively slowly with system size. Therefore, within this regime, we are able to count the exact number of solutions within a large search space that is intractable via direct enumerations.

The rest of the paper is organized as follows. We first briefly introduce the tensor network representation of generic vertex models on a square lattice in Sec. II. Section III describes the ICD algorithm and for coarse-graining and efficiently contracting the tensor network. As a warmup exercise, in Sec. IV we apply the ICD algorithm to the case of the six- and eight-vertex models, and compute the entropy *per* vertex, recovering the exact

results by extrapolating to the thermodynamic limit. In Sec. V we apply the ICD method to reversible classical computational problems as encoded in the vertex model of computation introduced in Ref. [8], and present numerical scaling results. In this section, we also discuss a relation between the number of solutions of the computational problem and the maximum bond dimension of the tensor network from an entanglement perspective. Finally, we close with Sec. VI, where we outline future applications of our ICD algorithm to both computational and physics problems.

II. TENSOR NETWORK FOR VERTEX MODELS

We start by introducing the tensor network representation for a generic vertex model. In our formulation, discrete degrees of freedom reside on the *edges* of a regular lattice and they are coupled locally to their neighboring degrees of freedom. Couplings between degrees of freedom are denoted by *vertices*. The couplings at each vertex $n = 1, \dots, N_{\text{sites}}$, where N_{sites} denotes the total number of vertices, are encoded into a tensor $T[n]$ whose rank will depend on the connectivity of the lattice. Fixing the state at all edges incident to a vertex collapses the corresponding tensor to a scalar. For concreteness, let us consider the square lattice as an example, as shown in Fig. 1; generalizations to other types of lattices are straightforward. Each tensor $T[n]$ is therefore a rank-4 tensor $T[n]_{ijkl}$, where i, j, k, l denote bond indices.

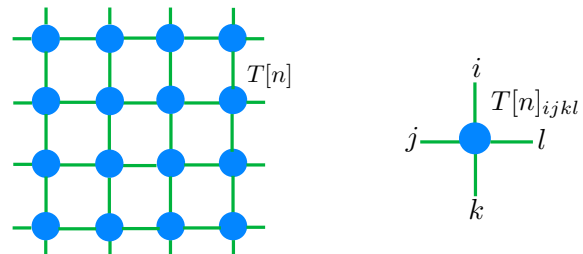


Figure 1. (Color online) Vertex model on a square lattice. A local tensor $T[n]_{ijkl}$ is defined on each lattice site.

The tensor representation is quite general. If, for example, one associates a Boltzmann weight with each combination of bond index values, one can encode statistical mechanics problems into the tensor network [17, 18, 21–24]. Alternatively, by assigning boolean 1s to “compatible” combinations of bond index values and boolean 0s to “incompatible” ones, such that the tensor represent a vertex constraint or a truth table, one can either study statistical mechanical vertex models (Sec. IV), or implement computational circuits with the tensor network (Sec. V). Finally, one could even embed the weights of a discretized path integral for a 1+1D quantum problem

in a two-dimensional network. For finite systems with boundaries, the boundary tensors will have a different rank from the bulk tensors.

We define the tensor trace of the network as

$$Z = \text{tTr} \prod_n T[n]_{ijkl}, \quad (1)$$

where n runs over all lattice sites and tTr denotes full contractions of all bond indices. This trace may correspond to the partition function for the 2D classical system, or the number of possible solutions of a computation, or the imaginary-time path integral for a 1D quantum system, etc. In general, a brute-force evaluation of the full tensor trace multiplies the dimensions of the tensors, thereby requiring a number of operations exponential in system sizes. It is therefore expedient for any strategy of evaluating the trace to keep the dimensions of tensors under control at intermediate steps, so that the tensor trace can be ultimately taken. Ideally, one would like a protocol that uses all available information — such as boundary conditions, compatibility constraints, energy costs or Boltzmann weights, depending on the particular problem at hand — to compress the tensor network as much as possible, while maintaining all the essential information therein. In Sec. III, we propose an efficient iterative scheme that achieves this goal. In particular, as we detail in Secs. IV and V, it provides a simple way to deal with finite systems without translational invariance, and subject to various types of boundary conditions.

III. COMPRESSION-DECIMATION ALGORITHM

In this section, we describe the compression-decimation algorithm that facilitates the exact contraction of tensor networks. The algorithm consists of two steps. First, we perform *sweeps* on the lattice via a singular value decomposition (SVD) of pairs of tensors in order to eliminate short-range entanglement and propagate information from the boundary to the bulk, hence removing the redundancies in the bond dimensions. Due to its nature, we call this step *compression*. Next, we contract pairs of rows and columns of the lattice such that the system size is reduced. This step is referred to as *decimation*. The two steps are then repeated until the size and bond dimensions of the tensor network become small enough to allow an exact full contraction of the network.

We emphasize that the sweeping is a key novelty of our scheme that has been missing in previous tensor network-based algorithms. Locally, the sweeps remove redundancies due to either short-range entanglement or incompatibility in the local tensors, and compress the information into tensors with smaller bond dimensions. Globally, the sweeps propagate information about the boundary conditions to the bulk, thus imposing global constraints on the

local bulk tensors. Moreover, since the sweeping is performed back and forth across the entire lattice, it does not differentiate between whether or not translational invariance is present. Therefore, our scheme may be adapted as a higher dimensional analog of the finite-system DMRG algorithm that applies to generic vertex models on finite lattices.

A. Compression

In this step, we visit sequentially each bond in the lattice and contract the corresponding indices of the two tensors sharing this bond. We then perform an SVD on the contracted bond and truncate the singular value spectrum keeping only those greater than a certain threshold δ . After that, the tensors are reconstructed with a smaller bond dimension. We define each forward plus backward traversal of all the bonds in the network as one *sweep*. The specific choice of the threshold δ depends on the desired precision, as well as the problem we are dealing with. For example, in formulating TNRG algorithms, δ can be chosen to be some small but finite number. On the other hand, for computational problems such as counting, δ is usually chosen to be zero within machine precision. We shall give concrete examples of both scenarios in Secs. IV and V.

Let us take two tensors with the shared bond labeled by i , $T[1]_{a_1 a_2 a_3 i}$ and $T[2]_{b_1 i b_2 b_3}$, as shown in Fig. 2a, where we denote the dimension of bond i as d_i .

We would like to reduce the dimension of bond i via SVD. In principle, this can be achieved by directly contracting $T[1]$ and $T[2]$ along dimension i into a matrix $M_{A,B} = T[1]_{A,i} T[2]_{i,B}$, where we have grouped the other three indices of each tensor into superindices $A \equiv (a_1 a_2 a_3)$ and $B \equiv (b_1 b_2 b_3)$, and then performing an SVD. However, to avoid decomposing the matrix $M_{A,B}$ with potentially large bond dimensions, we first do an SVD on each individual tensor (Fig. 2b):

$$T[1]_{A,i} = U[1]_{A,r} \Lambda[1]_r V[1]_{r,i}^\top, \quad (2a)$$

$$T[2]_{i,B} = U[2]_{i,r'} \Lambda[2]_{r'} V[2]_{r',B}^\top. \quad (2b)$$

Notice that the contraction of $T[1]$ and $T[2]$ can then be written as

$$T[1]T[2] = U[1]_{A,r} \left[\Lambda[1]_r V[1]_{r,i}^\top U[2]_{i,r'} \Lambda[2]_{r'} \right] V[2]_{r',B}^\top. \quad (2c)$$

This implies that we can instead perform an SVD on the part shown within brackets in Eq. (2c): $\widetilde{M}_{r,r'} = \Lambda[1]_r V[1]_{r,i}^\top U[2]_{i,r'} \Lambda[2]_{r'}$, which has much smaller dimensions since $d_r \leq \min(d_A, d_i)$, $d_{r'} \leq \min(d_B, d_i)$. Now we perform an SVD on the matrix $\widetilde{M}_{r,r'}$ to obtain (Fig. 2c)

$$\widetilde{M}_{r,r'} = U_{r,s} \Lambda_s V_{s,r'}^\top. \quad (2d)$$

(At each SVD step described above, we discard singular values that are smaller than δ .) Therefore, after the

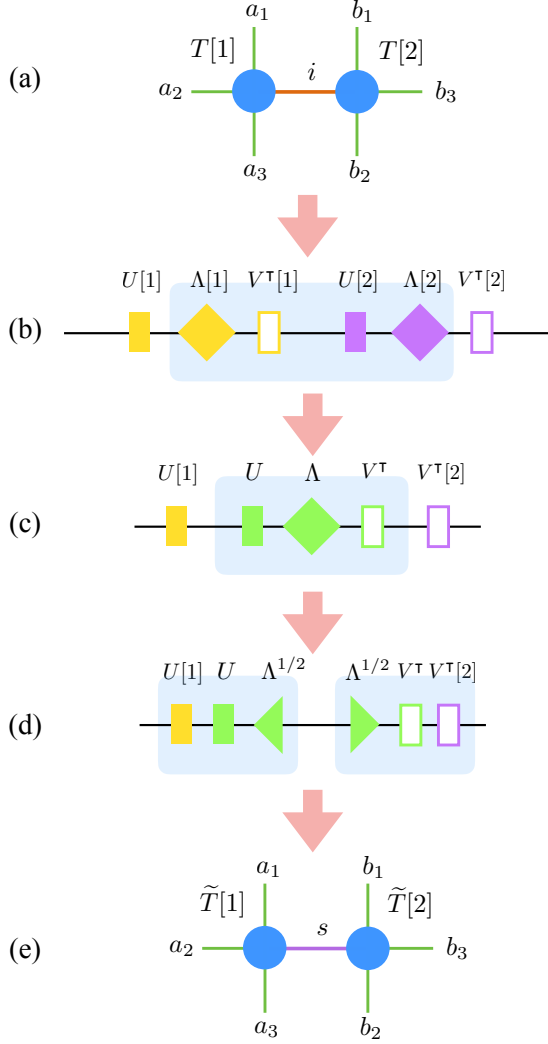


Figure 2. (Color online) The contraction-decomposition step in the sweeping. (a) Two tensors $T[1]$ and $T[2]$ sharing a bond i . (b) Perform SVDs on individual tensors respectively. (c) Perform an SVD on the shaded part. (d) Split the resultant matrices into two pieces. (e) Construct new tensors $\tilde{T}[1]$ and $\tilde{T}[2]$.

above steps, the bond dimension $d_s \leq \min(d_r, d_{r'}) \leq \min(d_i, d_A, d_B)$. Finally, we construct new tensors as

$$\tilde{T}[1]_{a_1 a_2 a_3 s} \equiv \tilde{U}_{(a_1 a_2 a_3), s} (\Lambda_s)^{1/2}, \quad (2e)$$

$$\tilde{T}[2]_{s b_1 b_2 b_3} \equiv (\Lambda_s)^{1/2} \tilde{V}_{s, (b_1 b_2 b_3)}^\tau, \quad (2f)$$

where the dimension of the shared bond is reduced (Fig. 2d,e). Starting from one boundary, we visit sequentially each bond $i \in 1, \dots, N_{\text{bonds}}$, where N_{bonds} is the total number of bonds in the lattice, and perform the steps outlined above, until we reach the opposite boundary. Then we repeat the procedure in the opposite direction, until we reach the original boundary. The sweeping can be repeated N_{sweeps} times, or until convergence of all bond dimensions.

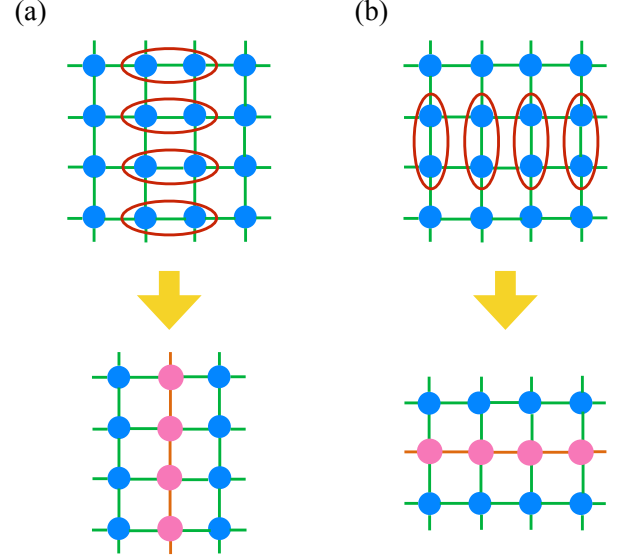


Figure 3. (Color online) (a) A column contraction involving pairs of tensors along the x direction. (b) A row contraction involving pairs of tensors along the y direction. The new tensors resulting from the contractions are denoted by pink dots, and the new bonds are denoted by orange lines.

B. Decimation

The second step of the algorithm is to contract pairs of rows and columns of the tensor network, so as to yield a lattice with a smaller number of sites [21, 23]. As we show in Fig. 3, this step consists of a column contraction (Fig. 3a), followed by a row contraction (Fig. 3b). In the column contraction, we contract pairs of tensors along the x direction, and obtain a new tensor (see also Fig. 2a):

$$\mathcal{T}_{(a_1 b_1) a_2 (a_3 b_2) b_3} = \sum_i T[1]_{a_1 a_2 a_3 i} T[2]_{b_1 i b_2 b_3}. \quad (3)$$

We then perform a row contraction similarly, during which pairs of tensors are contracted along the y direction.

During this step, the dimensions of the bonds perpendicular to the current direction of contractions are multiplied and hence will inevitably grow. Therefore, after all columns/rows are contracted, we sweep back and forth again to reduce the bond dimensions. A simplified version of the compression-decimation scheme is presented as pseudocode in Algorithm 1.

Algorithm 1 Iterative Compression-Decimation

Input: tensor network on a square lattice $\{T[n] | n \in 1, \dots, N_{\text{sites}}\}$; $N_{\text{sweeps}} \geq 1$; $\delta \geq 0$ (SVD truncation parameter).

Output: Z , as defined in Eq. (1)

```

1: repeat
2:   for  $i = 1, \dots, N_{\text{sweeps}}$  do (compression)
3:     for  $b = 1, \dots, N_{\text{bonds}}$  do (forward sweep)
4:       Contract, SVD, and update tensors as in Eq. 2
5:     end for
6:     for  $b = N_{\text{bonds}}, \dots, 1$  do (backward sweep)
7:       Carry out backward sweep similarly
8:     end for
9:   end for
10:  Perform column contractions by Eq.(3) (decimation)
11:  Perform row contractions similarly (decimation)
12: until network is decimated to single site
13: Carry out tensor trace Eq. (1)

```

A few remarks are in order. First, the lattice structure lends us more flexibility with the coarse-graining step since one does not have to contract every pair of rows and columns. For example, in cases of systems without translational invariance, representing either disordered statistical mechanics models or models encoding computational circuits, the bond dimensions are in general not distributed uniformly across the entire lattice. One could then perform the contractions selectively on rows and columns containing mostly tensors with small bond dimensions while leaving the rest for the next coarse-graining step. In practice, one could set an appropriate threshold in the algorithm depending on the specific problems. Second, the procedure described here is closely related to the TNRG algorithms where the key is to optimally remove short-range entanglement at each RG step. For example, Ref. [24] proposes a loop optimization approach for TNRG. An important step in that method is to filter out short-range entanglement within a plaquette via a QR decomposition, which we believe should be equivalent to our SVD-based sweeping. Moreover, the sweeps obviously take into account the effect of the environments of local tensors, but they are not limited to tree tensor networks as in Refs. 21 and 23. The loop structure of short-range entanglement is eliminated (at least partially, if not optimally) when we visit each bond around the loop and sweep across the whole system. Third, our procedure is more apt for systems without translational invariance, e.g., spin glasses. Finally, the computational cost of the compression-decimation algorithm scales as $O(\chi^5)$ — essentially the cost of the SVD of the largest tensors — where χ is the maximum bond dimension of the tensors.

IV. PLANAR ICE AND EIGHT-VERTEX MODEL

As an exercise, we apply our algorithm to two statistical mechanics models known as the six-vertex model,

i.e., a planar version of spin ice [30–33], and the eight-vertex model [34]. These models are defined as follows. Imagine we put Ising-like degrees of freedom on the links of a square lattice, where each link can take two possible states (“in” and “out”, or “+1” and “−1”). Then, at each vertex, we impose a constraint on the configurations of the four links emanating from the vertex. In Fig. 4 we show all configurations on the links allowed by the vertex constraint of both models.

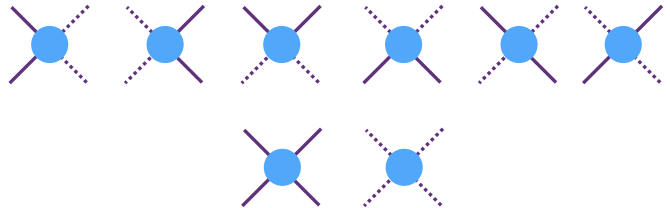


Figure 4. (Color online) The configurations of the link states allowed by the vertex constraints. The two link states are denoted by solid and dotted lines. For the planar ice model, the six configurations in the first row are allowed by the ice rules. For the eight-vertex model, the two additional configurations in the second row are also allowed by the \mathbb{Z}_2 Gauss law condition.

The two states on each link are denoted by solid and dotted lines. The first row of Fig. 4 corresponds to the allowed configurations in the planar ice model, known as the ‘ice rules’. In the eight-vertex model, the two additional configurations in the second row of Fig. 4 are also allowed. The eight-vertex model naturally appears as the physical space satisfying the Gauss law condition of a \mathbb{Z}_2 lattice gauge theory. Both models have an extensive zero-temperature entropy. We show below that our algorithm allows for an efficient counting of the number of satisfying configurations of both models, for given boundary conditions. Therefore, the entropies of the classical ground states can be efficiently computed for large but finite systems.

For convenience, we define planar ice and the eight-vertex model on a tilted square lattice of size $N = L \times W$, as depicted in Fig. 5a, where we take periodic boundary conditions along the vertical direction and open boundary conditions along the horizontal direction, i.e., the system is defined on a cylinder.

In order to represent the partition function of the vertex models as a tensor network, we define a local tensor for each vertex T_{ijkl} as shown in Fig. 6. Notice that in Fig. 5a, vertices at the boundary have only two neighbors. Therefore, tensors associated with boundary vertices have rank two: T_{ij} . The tensor indices label the degrees of freedom on the links, and each link has two possible states denoted as $i = 0, 1$. The tensor components are initialized in the following way: $T_{ijkl} = 1$ if the link configuration satisfies the vertex constraint; and $T_{ijkl} = 0$ otherwise. For example, in planar ice, $T_{ijkl} = 1$ if and only if there are two 1’s and two 0’s in the tensor

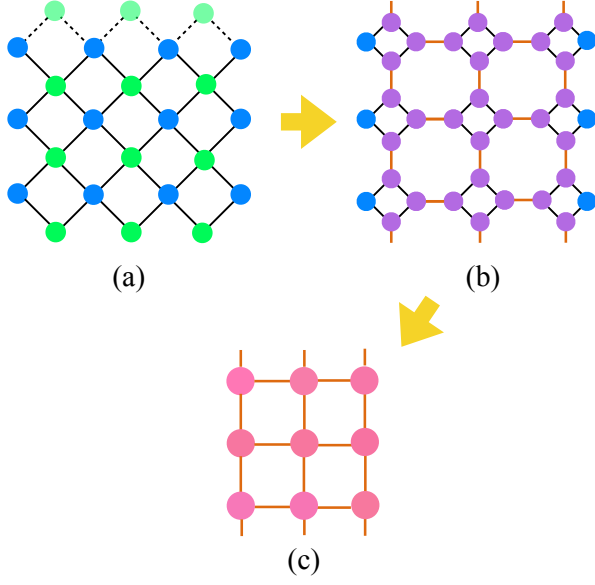


Figure 5. (Color online) Illustration of the local moves which turn the original lattice into a square lattice rotated by 45° . In (a), sites belonging to sublattice A and B are shown in blue and green dots, respectively. From (b) to (c), four sites belonging to a diamond are contracted into one.

indices. The tensors at the boundary can be initialized by taking the rank-4 tensor and summing over two of its indices: $\tilde{T}_{kl} = \sum_{ij} T_{ijkl}$, as to allow for all possible configurations for open boundary conditions. Alternatively, one may as well fix the boundary tensors as to restrict the system to a certain magnetization sector.

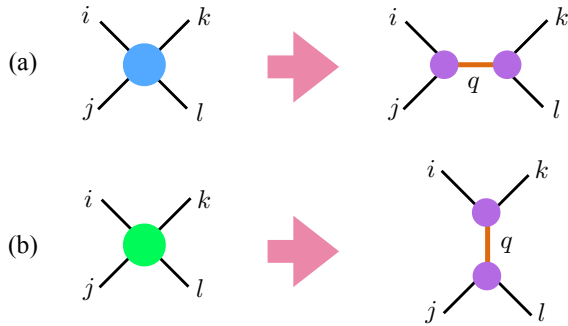


Figure 6. (Color online) Local moves that decompose each tensor on the original lattice into two along either horizontal or vertical direction, depending on whether the site belongs to sublattice A (a) or B (b).

Now we apply the algorithm outlined in Sec. III to this model. Since the vertex model is defined on a tilted square lattice, we first need to turn it into a lattice as shown in Fig. 1. This can be done by performing local moves on the tilted lattice, which we explain below.

The tilted square lattice Fig. 5a is bipartite, with two

sublattices A and B. Local tensor decompositions and contractions for tensors on each sublattice can rearrange the lattice into an “untilted” one, rotated by 45° with respect to the original lattice. We start by splitting each tensor on the original vertex lattice into two along either horizontal or vertical direction, depending on which sublattice the corresponding site belongs to. Let us take a bulk tensor T_{ijkl} on the original lattice. If the site belongs to sublattice A, we decompose the tensor horizontally into two rank-3 tensors, $T_{ijkl} = \sum_q A_{ijq} B_{klq}$; if the site belongs to sublattice B, we instead decompose the tensor vertically, $T_{ijkl} = \sum_q \tilde{A}_{ikq} \tilde{B}_{jlq}$, as shown in Fig. 6. Such a decomposition can be achieved via an SVD on the original tensors, $T_{(ij),(kl)} = U_{(ij),q} \Lambda_q V_{q,(kl)}^\top$ to yield $A_{ijq} = U_{(ij),q} (\Lambda_q)^{1/2}$ and $B_{klq} = (\Lambda_q)^{1/2} V_{q,(kl)}^\top$. We visit each site and split the tensors in this way. This turns the tensor network into the structure shown in Fig. 5b. We then further contract four tensors in a diamond into one and finally arrive at a new square lattice rotated by 45° with respect to the original one (Fig. 5c). With these local moves, which have to be carried out only once, we cast the problem into the form discussed in Sec. II.

We start by describing our results for the planar ice. This system has an extensive zero-temperature entropy due to the frustration induced by the ice rules. In the thermodynamic limit, the ground state entropy S was calculated exactly by Lieb [30]: $S/Nk_B = \frac{3}{2} \log_2 \frac{4}{3}$. This result was obtained for systems with periodic boundary condition in both directions, and is exact only in the infinite system limit. For our finite systems defined on a cylinder, there are finite-size corrections. Therefore, in order to benchmark against the exact solution, we do a finite-size scaling analysis.

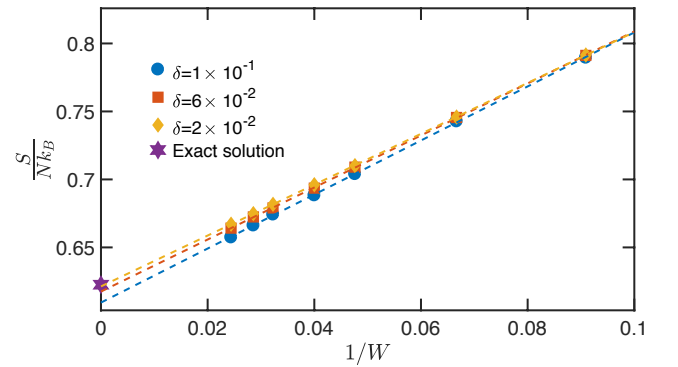


Figure 7. (Color online) The entropy density of the planar ice model as a function of $1/W$ for different truncation thresholds δ . The purple star on the vertical axis denotes the exact solution. One can see that as δ decreases, the extrapolated value in the thermodynamic limit approaches the exact solution.

In Fig. 7, we plot the entropy density as a function of $1/W$ for different choices of truncation threshold δ . One can see that, as δ decreases, the extrapolated value approaches the exact solution in the thermodynamic limit,

demonstrating that our algorithm, especially the sweeping, is capable of imposing the constraints at different length scales and yields the correct counting of satisfying configurations. Moreover, the error induced by raising the truncation threshold is relatively small, yet the computational cost of the algorithm is greatly reduced upon raising δ .

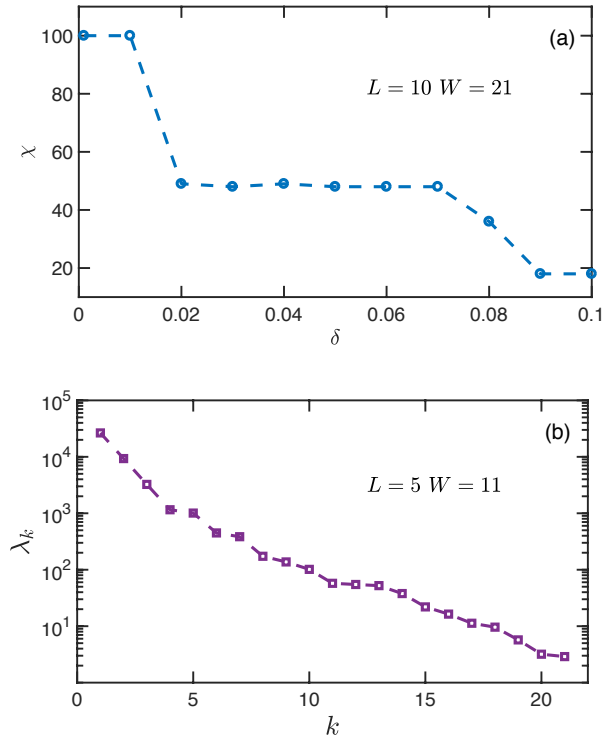


Figure 8. (Color online) (a) The maximum bond dimension during the compression-decimation steps of the algorithm as a function of the truncation threshold δ , for a system size $L = 10, W = 21$. (b) The singular value spectrum of a typical bond at an intermediate compression-decimation step, for a system size $L = 5, W = 11$ and $\delta = 10^{-4}$. The singular values decay nearly exponentially.

As shown in Fig. 8a, the maximum bond dimension during the compression-decimation steps decreases substantially as δ is increased from 10^{-4} to 10^{-1} . Within the range of system sizes shown in Fig. 7, the maximum bond dimensions for $\delta = 10^{-1}$ fluctuate around $\chi \approx 20$. This result implies that the singular value spectrum of the planar ice model should decay very fast. Indeed, we find that the singular values of a typical bond decay nearly exponentially after a few compression-decimation steps (Fig. 8b).

Within our formulation, it is straightforward to impose other boundary conditions. For example, one could fix the incoming legs of the entire column on the left boundary to be all $+1$ or all -1 . This would uniquely fix the vertex states of all other columns, hence leading to a unique ground state. We have checked that our algorithm indeed produces this result upon imposing such

boundary conditions.

Let us now turn to the eight-vertex model. One can easily compute the ground state entropy density of the eight-vertex model to be $S/k_B = L(W + 2) = N + 2L$ for open boundary condition, and $S/k_B = LW = N$ for fixed boundary condition. This result is exact for any finite system size. In this case, our algorithm is able to give the correct result *exactly* with $\delta = 0$ within machine precision, with a maximum bond dimension $\chi = 2$.

V. RANDOM TOFFOLI VERTEX MODEL

In this section, we provide an example of a hard computational problem where our scheme can be applied to find solutions in cases that are otherwise intractable. The model we study here is the vertex model representation of reversible classical computations introduced in Ref. [8]. The model is defined on a square lattice of finite size with periodic boundary condition on the transverse direction, thus forming a cylinder. Depending on the specific computation, different types of boundary conditions are imposed in the longitudinal direction. In addition, this model does not have translational invariance since each vertex encodes a different gate of the computational circuit. This model can encode general computational problems, including ranges of hard instances, and serves as an excellent candidate to benchmark the performance of our scheme.

We start by giving a self-contained review of the vertex model encoding reversible classical computations and construct its tensor network representation. A more in-depth discussion of the vertex model is given in Ref. [8].

A. The model

Any Boolean function can be implemented using a reversible circuit constructed out of TOFFOLI gates, which are reversible three-bit logic gates taking the inputs (a, b, c) to $(a, b, ab \oplus c)$. To facilitate the coupling of far-away bits while maintaining the locality of TOFFOLI gates, we use two-bit SWAP gates to swap neighboring bits, $(a, b) \rightarrow (b, a)$, until pairs of distant bits are adjacent to one another. Bits that do not need to be moved are simply copied forward using two-bit Identity (ID) gates. To obtain a plane-covering tiling and thus a square-lattice representation of the circuit, we combine the SWAP and ID gates into the three-bit gates (ID-ID, ID-SWAP, SWAP-ID, SWAP-SWAP) and represent each of them as well as the TOFFOLI gate as a vertex with three inputs and three outputs. The five types of vertices are shown in Fig. 9, with the input and output bits explicitly drawn on the links.

Alternatively, one can think of bits as spin $1/2$ particles located on the bonds between vertices, whereas each vertex imposes local constraints between “input” and “output” spins, such that only $2^3 = 8$ out of the $2^6 = 64$

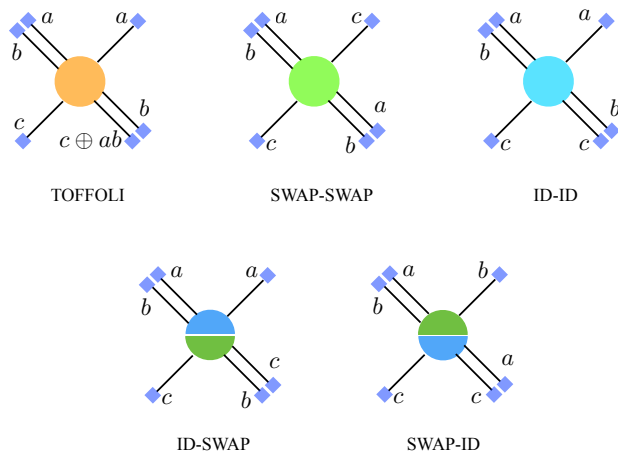


Figure 9. (Color online) Five types of vertices used for the vertex model representation of reversible classical computations. The input and output bits are denoted by blue squares on the links associated with a given vertex.

total configurations are allowed. For all five types of vertices, one can write local one- and two-spin interaction terms, such that the allowed configurations are given by the ground-state manifold of the Hamiltonian comprised of all these terms [8]. The allowed configurations are then separated from the excited states by a gap set by the energy scale of the couplings. In the large-couplings limit, interactions can be equivalently thought of as constraints and one therefore needs only to consider the subspace where local vertex constraints are always satisfied.

Using the five types of vertices introduced above, one can map an arbitrary classical computational circuit onto a vertex model on a tilted square lattice, as shown in Fig. 10.

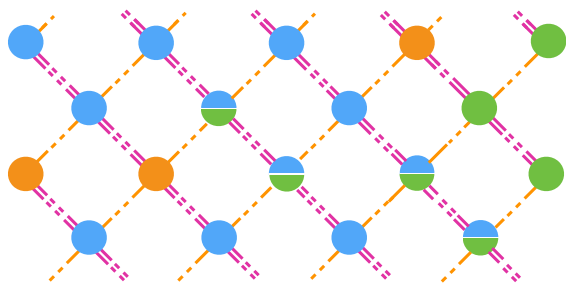


Figure 10. (Color online) Vertex model on a tilted square lattice encoding a generic classical computation. The left and right boundaries store the input and output states, and periodic boundary condition is taken along the transverse direction.

Bits at the left and right boundaries store the input and output respectively, and the horizontal direction corresponds to the computational “time” direction. The boundary condition along the transverse direction is cho-

sen to be periodic. Spin degrees of freedom representing input and output bits associated with each vertex are placed on the links. This model can be shown to display no thermodynamic phase transition irrespective of the circuit realizations via a straightforward transfer matrix calculation [8].

When either only the input or only the output boundary bits are fully determined a priori, the physical system functions as a regular circuit: the solution can be obtained by passing the boundary state through the next column of gates, obtaining the output, then passing this output on to the next column of gates, repeating the procedure until the other boundary is reached. This mode of solution, which we shall call *direct computation*, is trivial and its computational cost scales linearly with the area of the system.

On the other hand, by fixing only a subset of the left and right boundaries, a class of nontrivial problems can be encoded in the vertex model. For example, one can cast the integer factorization problem on a reversible multiplication circuit precisely in this way [8, 35]. In these cases, the boundary state cannot be straightforwardly propagated from the boundaries throughout the entire bulk, as the input or output of one or more gates is at most only partly fixed, and therefore direct computation unavoidably halts. Without any protocol of communication between the two partially fixed boundaries, one is left with trial-and-error enumeration of all boundary configurations, whose number grows exponentially with the number of unfixed bits at the boundaries. Even though it is sometimes possible to exploit special (nonuniversal) features of specific subsets of problems in order to devise efficient strategies of solution (e.g., factorization with sieve algorithms), general schemes that perform favorably in solving the *typical* instances in the encompassing class are important, both for highlighting the underlying universal patterns and as launchpads towards customized solvers for particular subsets of problems. The algorithm introduced in this work is of the latter general kind.

B. Tensor network representation

We shall now construct a tensor network representation of the vertex model, such that the full contraction of the tensors yields the total number of solutions satisfying the boundary conditions. In the statistical mechanics language, this is the partition function of the vertex model at zero temperature, which essentially counts the ground state degeneracy.

Bulk tensors. We define a rank-4 tensor associated with each vertex in the bulk, T_{ijkl} , as shown in Fig. 11a. The tensor components are initialized to satisfy the truth table of the vertex constraint, meaning that $T_{ijkl} = 1$ if $(ij) \rightarrow (kl)$ satisfies the vertex constraint, and $T_{ijkl} = 0$ otherwise. Here the indices should be understood as integers labeling the spin (bit) states on each bond. Notice that the indices i, l correspond to double bonds on the

lattice while j, k correspond to single bonds. Therefore, the original bond dimensions of the indices (i, j, k, l) are $(4, 2, 2, 4)$.

For concreteness, let us give an example of encoding the truth table of the TOFFOLI gate into the tensor T_{ijkl} . First, recall that the gate function of TOFFOLI is $(a, b, c) \rightarrow (a, b, d = c \oplus ab)$. Comparing Fig. 11a with Fig. 9, we identify on the input side, $i \equiv (ab) = 2^1b + 2^0a, j = c$; on the output side, $k = a, l \equiv (bd) = 2^1d + 2^0b$. In Table I, we explicitly list the truth table of the TOFFOLI gate and its corresponding non-zero tensor components. All unspecified tensor components are set to zero. Tensors encoding the other four types of vertex constraints can be obtained in a similar fashion.

input			output		tensor component	
a	b	c	a	b	d	$T_{ijkl} \equiv T_{(ab)ca(bd)}$
0	0	0	0	0	0	$T_{0000} = 1$
0	0	1	0	0	1	$T_{0102} = 1$
0	1	0	0	1	0	$T_{2001} = 1$
0	1	1	0	1	1	$T_{2103} = 1$
1	0	0	1	0	0	$T_{1010} = 1$
1	0	1	1	0	1	$T_{1112} = 1$
1	1	0	1	1	1	$T_{3013} = 1$
1	1	1	1	1	0	$T_{3111} = 1$

Table I. Truth table and the corresponding tensor components for the TOFFOLI gate. On the input side, $i \equiv (ab) = 2^1b + 2^0a, j = c$; on the output side, $k = a, l \equiv (bd) = 2^1d + 2^0b$. All unspecified components are zero.

Boundary tensors. The vertices at the boundary have only two bonds. Hence we define a rank-2 tensor T_{ij} at the boundary, where the indices i, j have the same meaning as the bulk tensors (Fig. 11b). Here we draw a distinction between boundary tensors whose vertex states are fixed and those that are not. For fixed boundary vertices, $T_{ij} = 1$ only for one component corresponding

to the fixed state, whereas for unfixed ones, $T_{ij} = 1 \forall i, j$.

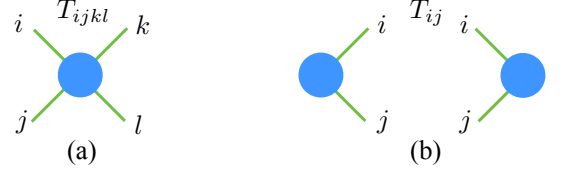


Figure 11. (Color online) Definition of (a) bulk and (b) boundary tensors.

Under the above definitions of local tensors, local compatibility between spins shared by two vertices is automatically guaranteed when contracting the corresponding two tensors. Moreover, the unfixed boundary tensors already encode the information of all possible vertex states in a compact way, fulfilling a form of classical virtual parallelization [15]. Therefore, the full contraction of the tensor network — if it can be performed — will give the total number of solutions subject to a certain boundary condition.

C. Entanglement and number of solutions

Before moving on to the concrete application of the algorithm, let us try to gain some insights into the bond dimensions of local tensors needed to encode the information of the total number of solutions from an entanglement point of view [36]. Let us denote the collection of free vertex states at the input and output boundaries by $\{q_{\text{in}}\}$ and $\{q_{\text{out}}\}$. We construct a weight $W(\{q_{\text{in}}, q_{\text{out}}\})$ which equals 1 if the state $\{q_{\text{in}}, q_{\text{out}}\}$ is a solution, and 0 otherwise. The partition function is then given by

$$Z = \sum_{\{q_{\text{in}}, q_{\text{out}}\}} W(\{q_{\text{in}}, q_{\text{out}}\}), \quad (4)$$

which equals the total number of solutions. Now we construct a *quantum* state as follows:

$$\begin{aligned} |\psi\rangle &= \sum_{\{q_{\text{in}}, q_{\text{out}}\}} W(\{q_{\text{in}}, q_{\text{out}}\}) |\{q_{\text{in}}, q_{\text{out}}\}\rangle \\ &= \sum_{\{q_{\text{in}}, q_{\text{out}}\}} \text{tTr} (T[1]^{q_{\text{in}1}} T[2]^{q_{\text{in}2}} \dots T[i] T[i+1] \dots T[N]^{q_{\text{out}L_{\partial}}}) |\{q_{\text{in}}, \{q_{\text{out}}\}\rangle, \end{aligned} \quad (5)$$

where N is the total number of vertices, L_{∂} is the number of unfixed vertices on each boundary, and tTr denotes tracing over all internal indices of the tensors. Let us imagine taking a cut perpendicular to the periodic direction and divide the system into two subsystems. The entanglement between subsystem left and

right is determined by the singular value spectrum of the *matrix* $\mathcal{W}(\{q_{\text{in}}\}, \{q_{\text{out}}\})$ reshaped from the weight $W(\{q_{\text{in}}, q_{\text{out}}\})$. \mathcal{W} is a matrix whose entries are either 1 or 0, and there can be at most one entry in each row and column that equals 1 due to the reversible nature of the circuit. Thus the rank of the matrix \mathcal{W} is Z , and

the zeroth-order Rényi entropy $S^{(0)} = \ln Z$. The entanglement entropy of the quantum state (5) is hence upper bounded by $S^{(1)} \leq S^{(0)} = \ln Z$. Therefore, at least when there is only a small (nonextensive) number of solutions, the amount of entanglement is low and the information can be encoded in tensors with small bond dimensions.

It may seem from the above argument that in the opposite limit of a large (extensive) number of solutions, the bond dimensions would necessarily be large. However, this is not true in general. Consider the open boundary condition under which every locally compatible configuration is a solution. In this extreme limit, the quantum state (5) is an equal amplitude superposition of all configurations, i.e., a product state. Such a state can be represented with tensors of bond dimension one in the ‘ x -basis’. One thus expects that in cases of many solutions, the state should also be close to a product state with low entanglement, and hence can be represented with tensors of small bond dimensions. The above arguments indicate that, if there is a highly entangled regime where the bond dimensions required to represent the solution are large, then it must necessarily be for systems with an intermediate number of solutions. In Sec. VE, we show numerically that, even in the intermediate regime where the solutions of an arbitrary vertex model are more than just a few, it is possible to obtain an efficient and compressed tensor network representation of the allowed-configuration manifold.

Having argued that the solutions of vertex models with partially fixed boundaries can be encoded into tensor networks with small bond dimensions, we set out to find this tensor-network representation. The pertinent motivating question is: given that there is a representation that can compress the full information of all solutions with relatively small bond dimensions, how can we find it efficiently?

D. Applying the ICD scheme

1. Local moves

To apply our algorithm in Sec. III to the random TOF-FOLI vertex model, we need to perform local moves on the tilted square lattice similar to that shown in Fig. 5. However, instead of doing an SVD on the original tensor as in Sec. IV, here we can use the fact that the tensors encode the truth tables of reversible gates and use an alternative method. Define a new set of tensors with an auxiliary index $q = 0, 1, \dots, 7$ labeling the vertex state, \tilde{T}_{ijkl}^q . Now the component of this rank-(4,1) tensor is one if and only if q is the same as the input state labeled by (i, j) . Then, the desired decomposition can be achieved

as follows:

$$\begin{aligned} A_{ijq} &= \sum_{kl} \tilde{T}_{ijkl}^q, & B_{klq} &= \sum_{ij} \tilde{T}_{ijkl}^q, \\ \tilde{A}_{ikq} &= \sum_{jl} \tilde{T}_{ijkl}^q, & \tilde{B}_{jlq} &= \sum_{ik} \tilde{T}_{ijkl}^q. \end{aligned} \quad (6)$$

One can easily check that the contraction of the A and B tensors gives back the original tensor T , and hence this achieves the splitting shown in Fig. 6. The remaining steps of the algorithm are carried out exactly in the same way as before. By construction, the bonds between the resulting bulk tensors all have dimension 8.

2. Control of bond dimensions

We can now apply the compression-decimation algorithm to count the number of solutions for a given boundary condition. As we discuss in Sec. III A, a truncation threshold δ needs to be specified in the sweeping step of the algorithm. Since we are doing an *exact* counting, no approximation in the truncation of the bond dimensions is made during the coarse-graining procedure, i.e., we choose $\delta = 0$ within machine precision. As mentioned earlier, from a statistical mechanics point-of-view, what we are computing is the zero-temperature partition function of the vertex model, which yields the ground state degeneracy. In the bulk, all locally compatible configurations are equally possible until they receive information from the boundary conditions. Therefore, the coarse-graining step effectively brings the boundaries close to one another, and the sweeping step propagates information from the boundary to the bulk and knocks out states encoded in local tensors that are incompatible with the global boundary conditions.

The reason why the growth of bond dimensions is controllable is that longer-range compatibility constraints over increasingly larger areas are enforced upon the coarse-grained tensors. These constraints are propagated to neighboring coarse-grained tensors upon sweeping, thus further reducing bond dimensions and compressing the tensor-network representation. For the trivial cases of either fixing all gates on one boundary or leaving them all free (open boundary condition), we have checked that the tensors converge to bond dimension one (scalars) after one sweep, *without the need of coarse-graining*. The tensor contraction is then simply reduced to multiplications of scalars, which can be trivially computed and indeed gives the correct counting. This demonstrates that the sweeping is responsible for propagating information from the boundary, and that the case of fully fixing one boundary is thus equivalent to direct computation, as described in Sec. VA.

In cases of mixed boundary conditions, the sweeping on the original lattice scale will generally not be sufficient to propagate information across the whole system or establish full communications between the two boundaries.

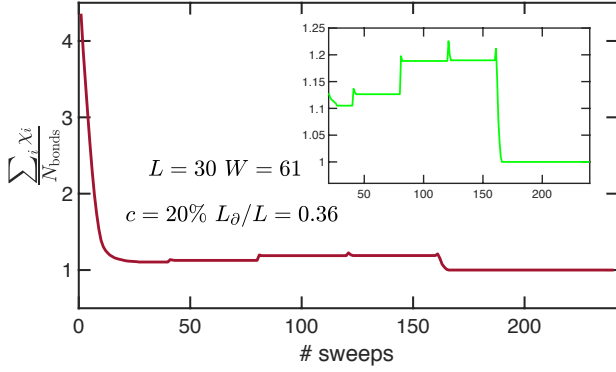


Figure 12. (Color online) The average bond dimension of the entire lattice as a function of the number of sweeps in the compression-decimation steps. The bumps where the average bond dimension increases slightly correspond to the points where we coarse-grain the lattice via column and row contractions. Inset: zoom-in plot from the 20th sweeping step.

Thus one would expect that while the bond dimensions close to the boundary may be small, those deep in the bulk may be large. We therefore perform the contractions selectively on rows and columns containing mostly tensors with small bond dimensions while leaving the rest for the next coarse-graining step, as described in Sec. III.

E. Numerical results

The computational cost of the ICD algorithm is determined by the maximum bond dimension encountered during the coarse-graining and sweeping procedures. In this section, we study the scaling of the maximum bond dimension as function of the set of parameters defining an instance of the problem: the number of vertices in each column L , the total number of columns (circuit depth) W , the concentration of TOFFOLI gates c , and the number of unfixed boundary vertices L_0 . For a given set of parameters, we consider random tensor networks corresponding to typical instances of the problem. By looking at the scaling of the bond dimensions, we gain some understanding of how the hardness of the problems depends on various parameters, which may serve as a guidance for designing and analyzing computational circuits for practical problems.

Before looking into the scaling of the maximum bond dimensions, we first show the average bond dimension for the entire lattice as a function of the number of sweeps in the compression-decimation steps. As seen from Fig. 12, the average bond dimension indeed decreases as the sweeping is performed. The bumps in the plot correspond to the points where we coarse-grain the lattice via column and row contractions. At a given length scale, the average bond dimension converges after a few sweeps. As we increase the length scales, the average bond dimension may first increase, but will eventu-

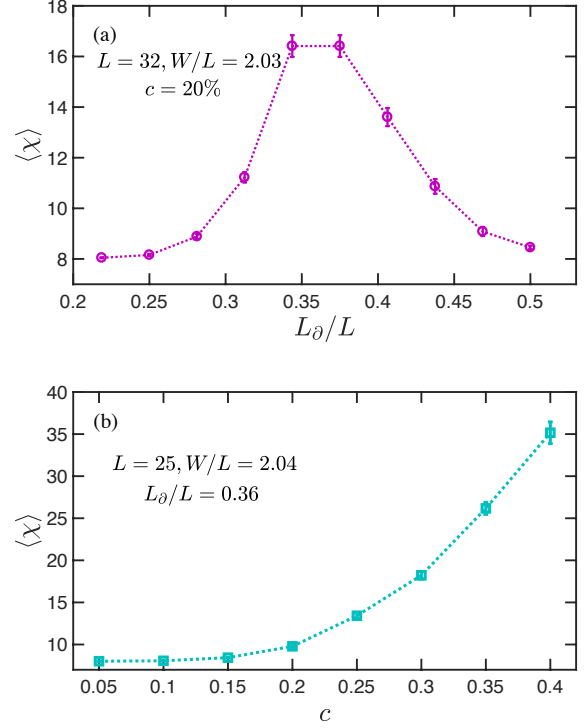


Figure 13. (Color online) Scaling of the maximum bond dimension χ with (a) the ratio of unfixed boundary vertices L_0/L , and (b) TOFFOLI concentration c . The remaining parameters are fixed in each plot. The data are obtained by averaging over 2000 realizations of random tensor networks.

ally drop again as we perform sweeps at the new length scale. This demonstrates that the sweeping is able to impose global constraints at the boundary into the bulk, hence keeping the bond dimensions of bulk tensors under control.

We expect the maximum bond dimension to follow the scaling function $\chi = \mathcal{G}(L_0/L, c, L, W/L)$. Below we study the growth of maximum bond dimensions as a function of each system parameter numerically. First, we consider the scaling of χ as the ratio of unfixed boundary vertices L_0/L is varied, with the other parameters fixed. As shown in Fig. 13a, the bond dimensions are small for both small and large L_0/L . This is in agreement with our discussions in Sec. VC, where we argued that in both regimes the states are close to product states and there should exist a representation in which the bond dimensions are small (the ‘ z -basis’ and ‘ x -basis’). For intermediate values of L_0/L , the bond dimensions grow, indicating the existence of a hard regime where either there is no such a representation of small bond dimensions to fully encode the solutions, or it is very hard to find such a representation via tensor optimization algorithms.

Fixing $L_0/L = 0.36$, which corresponds to the hard regime in Fig. 13a, we plot the scaling of χ as a function

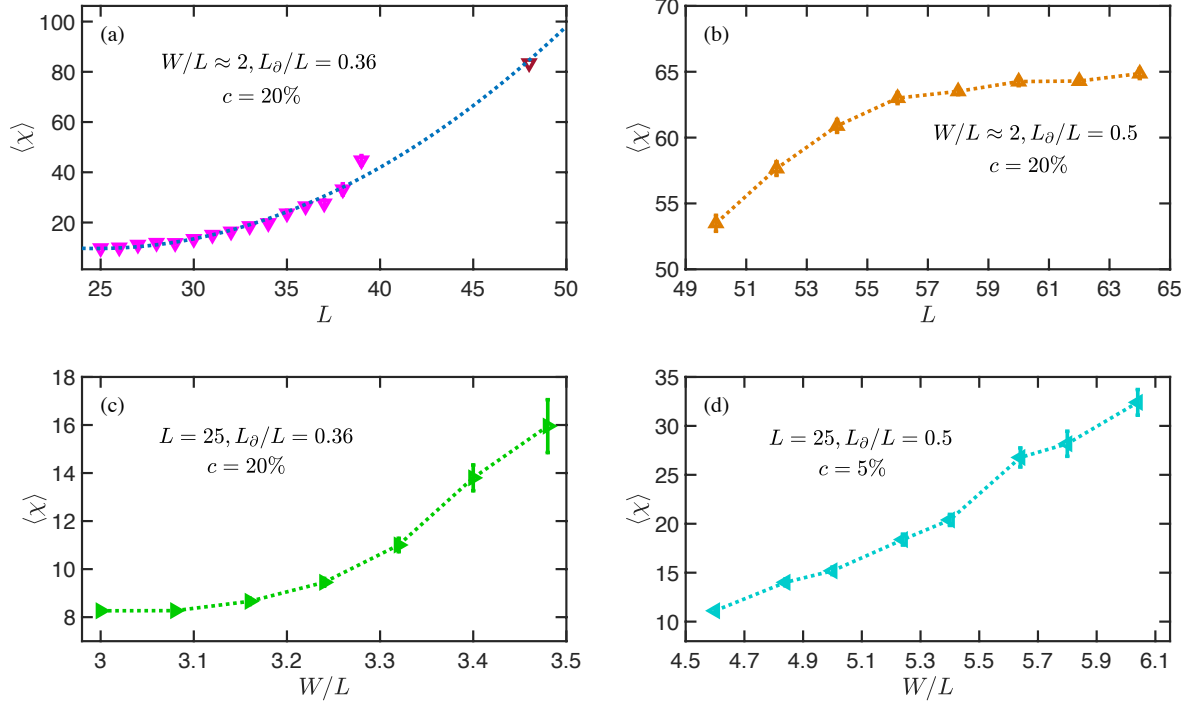


Figure 14. (Color online) Scaling of the maximum bond dimension χ with L (a,b) and W/L (c,d). The data are obtained by averaging over 500 to 2000 realizations of random tensor networks. In (a), the last point is averaged over 7 realizations and the error bar is not shown. The blue dotted line is a guide to the eye, and corresponds to a quadratic fitting.

of the TOFFOLI concentration c . The TOFFOLI gates impose nontrivial vertex constraints, which involve a non-linear relationship between the input and output bits. In fact, in the absence of TOFFOLI gates, the vertex model can be expressed as $3L$ decoupled one-dimension Ising chains whose dynamics are simple [8]. In the ICD algorithm, the maximum bond dimension indeed grows with increasing TOFFOLI concentrations, as depicted in Fig. 13b.

Now let us look at the scaling of χ as a function of the input size L . Again, we fix $L_\theta/L = 0.36$ to stay in the hard regime. Figure 14a shows that the maximum bond dimension increases with increasing input size, even when the aspect ratio W/L of the circuit is fixed. Because of the limited range of L we were able to analyze, we cannot draw any conclusion regarding the functional form of this scaling, which would determine the complexity of our algorithm. However, we can demonstrate that our algorithm is able to solve the problem in regimes that are still intractable using a naive enumeration of solutions. For this purpose, we move away from the hardest regime and choose $L_\theta/L = 0.5$. As can be seen in Fig. 14b, we are able to reach much larger values of L in this regime, and the bond dimensions, although still growing, increase at a much slower pace. In fact, we were able to reach $L = 96$ with an average maximum bond dimension $\langle \chi \rangle = 78.25$ (data not shown). Since half of

the input vertices are unknown, a direct trial-and-error enumeration would take $8^{48} \approx 10^{43}$ iterations to perform an exact counting, which is prohibitive even with parallelization. We have thus shown that there is a subset of nontrivial problems that can easily be solved by the ICD method, for which (a) direct enumeration is impossible to scale up and (b) efficient custom algorithms are not known.

Finally, we show the scaling with the aspect ratio W/L . As we previously discussed, the key to the reduction of the bond dimensions of bulk tensors is the global constraint imposed at the boundary. The coarse-graining step brings the boundaries close together while the sweeping step helps propagate information. Therefore, one should expect the problem to become harder as the circuit depth W increases for a fixed L , since it takes more iterations of coarse-graining for the connection between the boundaries to be built, all the while the bond dimensions of the bulk tensors barely decrease. In Fig. 14c we show the scaling of χ as a function of W/L in the hard regime; χ indeed grows upon increasing W/L , as expected. For computational problems of practical interests, the vertex model representation often has the feature of low TOFFOLI concentration but large aspect ratio, e.g., the multiplication circuit [8, 35]. In Fig. 14d we show data for cases with this feature by lowering the TOFFOLI concentration to $c = 5\%$ and keeping

$L_\partial/L = 0.5$. We find that the bond dimensions grow in a similar fashion as in Fig. 14c, although a larger range of values of W/L now becomes amenable.

The maximum bond dimension is not the only quantity that determines the performance of our algorithm. Unlike the TNRG algorithms, where the bond dimensions of all tensors and all tensor legs are uniform by choice, here the bond dimensions of different tensors and different legs of a single tensor are highly nonuniform. One could imagine cases where χ is large but only in one of the legs of a tensor, versus cases where χ is smaller but it appears in all four legs of a tensor. The former is more efficiently solved using the ICD algorithm in spite of the larger χ . Therefore, the distribution of χ throughout the system is also an important factor that can be further exploited to improve the performance of ICD.

VI. SUMMARY AND OUTLOOK

We presented a method for contracting tensor networks that is suited for vertex models with arbitrary boundary conditions and with or without translation invariance. The technique was motivated by the necessity of carrying out the tensor traces in statistical physics vertex models of classical computation. In that case the tensor trace represents the number of solutions, from which explicit solutions can be found efficiently when the number of solutions is small. However, the method applies generically to any system, classical or quantum, whose quantity of interest is a tensor trace in an arbitrary lattice.

Our scheme consists of iteratively compressing tensors through a contraction-decomposition operation that reduces their bond dimensions, followed by decimation, which increases bond dimensions but reduces the network size. By repeated applications of this two step process – compression followed decimation – one can gradually collapse rather large tensor networks.

In the context of computation, the method allowed us to study relatively large classical reversible circuits represented by two dimensional vertex models. By contrast with thermal annealing, direct computation from a fully specified input boundary through the use of tensor networks occurs in a time linear in the depth of the circuit. For complex problems with partially fixed input/output boundaries tensor networks enable us to count solutions in problems where enumeration would otherwise take of order 8^{50} operations.

We close with an outlook of future directions motivated by this work.

First, focusing on the method *per se*, the performance

of our ICD algorithm could still be further improved. There are enhancements that are simply operational in nature, such as parallelization of the sweeping step of the algorithm, which can be accomplished by dividing the tensors into separate non-overlapping sets.

Second, at a more fundamental level, as we point out at the end of Sec. V E, a better understanding of the mechanism by which short-range entanglement is removed within the ICD method would require a systematic study of the evolution of the spatial distribution of bond dimensions. The goal is to design more controlled bond dimension truncation schemes that also involve the effect of the environment of local tensors, as proposed in Refs. [19, 21, 23, 24]. More generally, we expect that our method can be applied to both classical and quantum many-body systems in two and higher dimensions.

Third, in our study of computation-motivated problems, we focused on random tensor networks corresponding to random computational circuits. However, the ICD methodology should be used to address problems of practical interest, a research direction that is being currently explored. The results on the scaling of the bond dimensions presented above should inform the design and analysis of tractable computational circuits, such as circuits with $W \sim L$ and a moderate number of TOFFOLI gates. Multiplication circuits based on partial sums, for instance, are very dense in TOFFOLI gates, and hence are not *a priori* candidates for tensor network formulations of related problems, such as factoring. However, different multiplication algorithms whose associated vertex models are less dense in TOFFOLI gates, and other computational problems could be amenable by our approach. Identifying classes of computational problems of practical interest that can be tackled with tensor network methods remains an open problem at the interface between physics and computer science.

Finally, from a statistical mechanics point-of-view, one may speculate that the ICD algorithm could allow us to study the glass phase of disordered spin systems for which classical Monte Carlo dynamics breaks down due to loss of ergodicity.

ACKNOWLEDGMENTS

We thank Justin Reyes, Oskar Pfeffer, and Lei Zhang for many useful discussions. The computations were carried out at Boston University’s Shared Computing Cluster. We acknowledge the Condensed Matter Theory Visitors Program at Boston University for support. Z.-C. Y. and C. C. are supported by DOE Grant No. DE-FG02-06ER46316.

[1] M. Mézard, G. Parisi, and R. Zecchina, *Science* **297**, 812 (2002).

[2] M. Mézard and A. Montanari, *Information, physics, and computation* (Oxford Univer-

- sity Press, 2009).
- [3] F. Ricci-Tersenghi, *Science* **330**, 1639 (2010).
 - [4] T. Jörg, F. Krzakala, G. Semerjian, and F. Zamponi, *Phys. Rev. Lett.* **104**, 207206 (2010).
 - [5] A. P. Young, S. Knysh, and V. N. Smelyanskiy, *Phys. Rev. Lett.* **104**, 020502 (2010).
 - [6] I. Hen and A. Young, *Phys. Rev. E* **84**, 061152 (2011).
 - [7] E. Farhi, D. Gosset, I. Hen, A. W. Sandvik, P. Shor, A. P. Young, and F. Zamponi, *Phys. Rev. A* **86**, 052334 (2012).
 - [8] C. Chamon, E. Mucciolo, A. Ruckenstein, and Z.-C. Yang, *Nat. Commun.* **8** (2017).
 - [9] A. Cichocki, arXiv preprint arXiv:1403.2048 (2014).
 - [10] N. Vervliet, O. Debals, L. Sorber, and L. De Lathauwer, *IEEE Signal Processing Magazine* **31**, 71 (2014).
 - [11] A. Cichocki, arXiv preprint arXiv:1407.3124 (2014).
 - [12] J. Biamonte, V. Bergholm, and M. Lanzagorta, *Journal of Physics A: Mathematical and Theoretical* **46**, 475301 (2013).
 - [13] J. D. Biamonte, J. Morton, and J. Turner, *Journal of Statistical Physics* **160**, 1389 (2015).
 - [14] J. Biamonte and V. Bergholm, arXiv preprint arXiv:1708.00006 (2017).
 - [15] C. Chamon and E. R. Mucciolo, *Phys. Rev. Lett.* **109**, 030503 (2012).
 - [16] F. Verstraete and J. I. Cirac, arXiv preprint cond-mat/0407066 (2004).
 - [17] M. Levin and C. P. Nave, *Phys. Rev. Lett.* **99**, 120601 (2007).
 - [18] Z.-C. Gu, M. Levin, and X.-G. Wen, *Phys. Rev. B* **78**, 205116 (2008).
 - [19] Z.-C. Gu and X.-G. Wen, *Phys. Rev. B* **80**, 155131 (2009).
 - [20] G. Evenbly and G. Vidal, *Phys. Rev. B* **79**, 144108 (2009).
 - [21] Z. Y. Xie, J. Chen, M. P. Qin, J. W. Zhu, L. P. Yang, and T. Xiang, *Phys. Rev. B* **86**, 045139 (2012).
 - [22] G. Evenbly and G. Vidal, *Phys. Rev. Lett.* **115**, 180405 (2015).
 - [23] H.-H. Zhao, Z.-Y. Xie, T. Xiang, and M. Imada, *Phys. Rev. B* **93**, 125115 (2016).
 - [24] S. Yang, Z.-C. Gu, and X.-G. Wen, *Phys. Rev. Lett.* **118**, 110504 (2017).
 - [25] M. Bal, M. Mariën, J. Haegeman, and F. Verstraete, *Phys. Rev. Lett.* **118**, 250602 (2017).
 - [26] H. J. Liao, Z. Y. Xie, J. Chen, Z. Y. Liu, H. D. Xie, R. Z. Huang, B. Normand, and T. Xiang, *Phys. Rev. Lett.* **118**, 137202 (2017).
 - [27] G. Evenbly, *Phys. Rev. B* **95**, 045117 (2017).
 - [28] A. M. Goldsborough and G. Evenbly, arXiv preprint arXiv:1708.07652 (2017).
 - [29] U. Schollwöck, *Rev. Mod. Phys.* **77**, 259 (2005).
 - [30] E. H. Lieb, *Phys. Rev.* **162**, 162 (1967).
 - [31] S. T. Bramwell and M. J. Gingras, *Science* **294**, 1495 (2001).
 - [32] C. Castelnovo, R. Moessner, and S. Sondhi, *Annu. Rev. Condens. Matter Phys.* **3**, 35 (2012).
 - [33] S. Kourtis and C. Castelnovo, *Phys. Rev. B* **94**, 104401 (2016).
 - [34] R. J. Baxter, *Exactly solved models in statistical mechanics* (Elsevier, 2016).
 - [35] V. Vedral, A. Barenco, and A. Ekert, *Phys. Rev. A* **54**, 147 (1996).
 - [36] C. Chamon and E. R. Mucciolo, *Journal of Statistical Mechanics: Theory and Experiment* **2013**, P04008 (2013).